Philosophical Magazine
Vol. 90, Nos. 1–4, 7–28 January 2010, 125–140

Taylor & Francis
Taylor & Francis Group

Phase-field model of multiferroic composites: Domain structures of ferroelectric particles embedded in a ferromagnetic matrix

P.P. Wu[ab]*, X.Q. Ma[a], J.X. Zhang[b] and L.Q. Chen[b]

[a]*Department of Physics, University of Science and Technology Beijing, Beijing 100083, China;* [b]*Department of Material Science and Engineering, The Pennsylvania State University, University Park, PA 16802, USA*

(*Received 19 January 2009; final version received 12 July 2009*)

The ferroelectric domain structures in 1-3 type bulk magnetoelectric composites were studied using the phase-field method. The ferroelectric polarization distributions in triangle, square, circle, and other polygons-shaped rods embedded in a ferromagnetic matrix were obtained. The influences of ferroelectric particle size and symmetry and the surrounding magnetic phase medium on the stability of double vortex structures are discussed.

Keywords: multiferroic composite; magnetoelectric composite; vortex structure; phase-field method

1. Introduction

Multiferroics are a class of materials that are simultaneously ferromagnetic and ferroelectric, and have potential applications in multifunctional devices, transducers, actuators and sensors [1–5]. There are two types of multiferroics: intrinsic magnetoelectrics that exist as a single-phase state, such as $YMnO_3$, $BiMnO_3$ and $BiFeO_3$, and extrinsic multiferroics that are composites or solid solutions of ferroelectric and ferromagnetic crystals. Since the number of intrinsic multiferroics is small [4], there have been many efforts to synthesize multiferroic composites [5–9].

For composites of ferromagnetic and ferroelectric crystals, the coupling between the ferromagnetic and ferroelectric order parameters is through the strain order parameter. In other words, the magnetostrictive and electrostrictive (or piezoelectric) effects of the ferromagnetic and ferroelectric crystals lead to a coupling between magnetization and polarization through the elastic interactions. In a composite, an applied magnetic field produces redistributions and changes in magnetization in the ferromagnetic phase, which in turn leads to redistributions of strains caused by the magnetostrictive effect. The strains imposed upon the ferroelectric (or piezoelectric) phase by the ferromagnetic phase through the magnetostrictive strain then results in changes in the polarization distributions and possibly switching in the ferroelectric

*Corresponding author. Email: pingpingwu-ustb@126.com

ISSN 1478–6435 print/ISSN 1478–6443 online

DOI: 10.1080/14786430903193266
http://www.informaworld.com

phase. Therefore, the coupling between the ferromagnetic and ferroelectric crystals through strain offers a possibility of switching electric polarization by a magnetic field or vice versa.

It is easy to see that the magnetoelectric coupling effect is directly proportional to the magnetostrictive and electrostrictive coefficients within the ferromagnetic and ferroelectric crystals as well as to the elastic constants. These material properties are fixed by choices of the individual constituent phases. However, the overall magnetoelectric effect is also critically dependent on the composite microstructure, i.e. the size, shape and spatial distributions of the phases in the composites.

Using the concept of phase connectivity [10], the phase distributions in a two-phase magnetoelectric composite can be described by the notations 0-3, 2-2, 1-3, etc. Recently, the magnetoelectric coupling phenomena have been studied for 1-3 type structured films [11] and bulk [12,13] magnetoelectric composites. Theoretical calculations [14] showed that the 1-3 type structured composites may produce significant magnetoelectric coupling.

Although our ultimate goal is to predict the magnetoelectric coupling effects as a function of composite microstructure, in this work we focus on the ferroelectric domain structures and polarization distribution of the 1-3 type bulk magnetoelectric composites. We employ the phase-field model, which has been used to study the physical properties of magnetoelectric composites [15] and thin films [16]. In particular, we studied the domain structures of square-, circle- and polygon-shaped ferroelectric $BaTiO_3$ rods embedded in a ferromagnetic matrix. In addition, we also studied square-shaped rods with different aspect ratios. The effect of magnetization orientation in the surrounding magnetic phase will also be discussed.

2. Phase-field model of multiferroic composites

In our phase-field model, we use three field variables to describe the domain structures in a two-phase ferroelectric and ferromagnetic composite. A phase field, $\eta(r)$, is introduced to describe the spatial distribution of the magnetic and ferroelectric phases in the composite. In the current implementation, the phase field is non-evolving, representing a static two-phase composite microstructure. If $\eta(r) = 1$, position r is occupied by the magnetic phase, whereas for $\eta(r) = 0$ it is the ferroelectric phase. Within the magnetic phase, the magnetic domain structure is represented by the local magnetization field, $\boldsymbol{M}$(r), whereas it is the local electric polarization field, $\boldsymbol{P}$(r), that describes the domain structures in the ferroelectric phase. The total free energy of a magnetoelectric composite includes magnetocrystalline anisotropy energy, magnetic exchange energy, magnetostatic energy, external magnetic field energy, ferroelectric bulk free energy, ferroelectric domain wall energy, electrostatic energy and elastic energy, i.e.

$$F = \int_V \left[\eta(r) f_{ferromagnetic} + (1 - \eta(r)) f_{ferroelectric} + f_{elast}\right] \mathrm{d}V, \tag{1}$$

where

$$f_{ferromagnetic} = K_1\left(m_1^2m_2^2 + m_1^2m_3^2 + m_2^2m_3^2\right) + K_2m_1^2m_2^2m_3^2 + A(\nabla_i m_i)^2 - \frac{1}{2}\mu_0 M_s H_i^d m_i - \mu_0 M_s H_i^a m_i, \tag{2}$$

$$f_{ferroelectric} = \frac{1}{2}\alpha_{ij}P_iP_j + \frac{1}{4}\gamma_{ijkl}P_iP_jP_kP_l + \frac{1}{6}\omega_{ijklmn}P_iP_jP_kP_lP_mP_n + \ldots + \frac{1}{2}G_{ijkl}P_{i,j}P_{k,l} - \frac{1}{2}E_i^dP_i - E_i^aP_i, \tag{3}$$

$$f_{elastic} = \frac{1}{2}c_{ijkl}\left(\varepsilon_{ij} - \lambda_{ijkl}m_km_l - Q_{ijkl}P_kP_l\right)\left(\varepsilon_{kl} - \lambda_{klij}m_im_j - Q_{klij}P_iP_j\right), \tag{4}$$

where m_i are the components of the unit magnetization vector, $\boldsymbol{m} = \boldsymbol{M}/M_s$, M_s is the saturation magnetization, K_1 and K_2 are the anisotropy constants, A is the exchange stiffness constant, $\boldsymbol{H}_d$ is the demagnetization field that is determined by the long-range interaction among the magnetic moments in the system, μ_0 is the permeability of vacuum, and $\boldsymbol{H}^a$ is the externally applied magnetic field where α_{ij}, β_{ijk}, γ_{ijkl} and ω_{ijklmn} are the phenomenological Landau expansion coefficients, G_{ijkl} is the tensor of the gradient energy coefficients, $P_{i,j} = \partial P_i/\partial x_j$, E_i^a is the ith component of an applied electric field, E_i is the ith component of internal electric field generated by the polarization distribution, c_{ijkl} and Q_{ijkl} are the elastic and electrostrictive constant tensors, respectively. All the coefficients are generally assumed to be independent of temperature except α_{ij}, which is linearly proportional to temperature, i.e. $\alpha_{ij} = \alpha_{ij}^o(T - T_o)$, where T_o is the Curie temperature.

To obtain spatial distribution of E_i, ε_{ij} and $\boldsymbol{H}_d$ in Equations (1)–(4), one has to solve the electrostatic, elasticity and magnetostatic equations for a given distribution of polarization, magnetization or eigenstrains, i.e.

$$\mathrm{div}[\boldsymbol{\kappa}\varepsilon_0 \cdot \boldsymbol{E}] = 0, \quad \mathrm{div}[\boldsymbol{c} \cdot (\boldsymbol{\varepsilon} - \boldsymbol{\varepsilon}^o)] = 0, \quad \mathrm{div}(\mu_o\boldsymbol{H}_d + \boldsymbol{M}) = 0, \tag{5}$$

where k_{ij} is the dielectric constant tensor and

$$\varepsilon_{ij}^o = Q_{ijkl}P_kP_l + \lambda_{ijkl}m_km_l. \tag{6}$$

With all the energetic contributions, the evolution of initially non-equilibrium order parameter fields towards equilibrium can be described by the time-dependent Ginzburg–Landau (TDGL) and Landau–Lifshits–Gilbert (LLG) equations (see, for example, [17]),

$$\frac{\partial P_i(\boldsymbol{r}, t)}{\partial t} = -L_P\frac{\delta F}{\delta P_i(\boldsymbol{r}, t)}, \tag{7}$$

$$\left(1 + g^2\right)\frac{\partial \boldsymbol{m}}{\partial t} = -\gamma_o\boldsymbol{m} \times \boldsymbol{H}_{eff} - \frac{\gamma_o g}{M_s}\boldsymbol{m} \times \left(\boldsymbol{m} \times \boldsymbol{H}_{eff}\right), \tag{8}$$

where L_P is kinetic coefficient related to domain wall mobility, γ_o is the gyromagnetic ratio, g is the damping constant and $\boldsymbol{H}_{eff}$ is the effective magnetic field,

$$\boldsymbol{H}_{eff} = -\frac{1}{\mu_o}\frac{\partial F}{\partial M}. \tag{9}$$

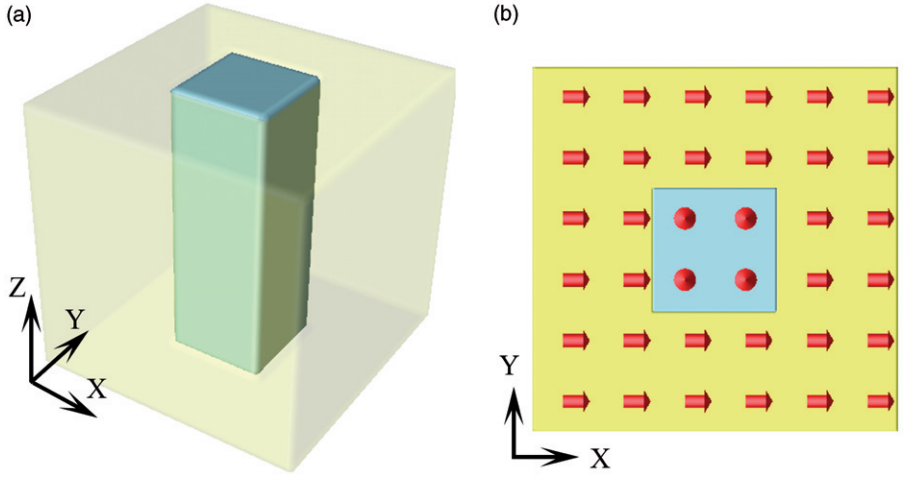

Figure 1. (Color online). (a) Three-dimensional (3D) schematic illustration of the magnetoelectric material in this work; a periodical boundary is employed. (b) A vector plot of the section plane of the 1-3 type magnetoelectric material.

3. Materials constants and simulation conditions

In this paper, as an example, we consider 1-3 type magnetoelectric composites made up of a ferroelectric $BaTiO_3$ rod embedded in a magnetic $CoFe_2O_4$ medium, as shown in Figure 1a. The free energy as a function of polarization for $BaTiO_3$ is described by an eighth-order polynomial [18,19],

$$\begin{aligned} f_{Land} = {} & \alpha_1(P_1^2 + P_2^2 + P_3^2) \\ & + \alpha_{11}(P_1^4 + P_2^4 + P_3^4) + \alpha_{12}(P_1^2P_2^2 + P_2^2P_3^2 + P_1^2P_3^2) \\ & + \alpha_{111}(P_1^6 + P_2^6 + P_3^6) + \alpha_{112}[P_1^2(P_2^4 \\ & + P_3^4) + P_2^2(P_1^4 + P_3^4) + P_3^2(P_1^4 + P_2^4)] + \alpha_{123}P_1^2P_2^2P_3^2 \\ & + \alpha_{1111}(P_1^8 + P_2^8 + P_3^8) + \alpha_{1112}[P_1^6(P_2^2 + P_3^2) + P_2^6(P_1^2 \\ & + P_3^2) + P_3^6(P_1^2 + P_2^2)] + \alpha_{1122}(P_1^4P_2^4 + P_2^4P_3^4 + P_1^4P_3^4) \\ & + \alpha_{1123}(P_1^4P_2^2P_3^2 + P_2^4P_1^2P_3^2 + P_3^4P_1^2P_2^2), \end{aligned} \tag{10}$$

where $\alpha_1 = 4.124(T - 115) \times 10^5\,C^{-2}\,m^2\,N$, $\alpha_{11} = -2.097 \times 10^8\,C^{-4}\,m^6\,N$, $\alpha_{12} = 7.974 \times 10^8\,C^{-4}\,m^6\,N$, $\alpha_{111} = 1.294 \times 10^9\,C^{-6}\,m^{10}\,N$, $\alpha_{112} = -1.950 \times 10^9\,C^{-6}\,m^{10}\,N$, $\alpha_{123} = -2.500 \times 10^9\,C^{-6}\,m^{10}\,N$, $\alpha_{1111} = 3.863 \times 10^{10}\,C^{-8}\,m^{14}\,N$, $\alpha_{1112} = 2.529 \times 10^{10}\,C^{-8}\,m^{14}\,N$, $\alpha_{1122} = 1.637 \times 10^{10}\,C^{-8}\,m^{14}\,N$, $\alpha_{1123} = 1.367 \times 10^{10}\,C^{-8}\,m^{14}\,N$, and the dielectric constant used in our simulation is $k_{11} = k_{22} = k_{33} = 500$. Smaller values of dielectric constants, from 1 to 300, were also employed to test the sensitivity of domain structures on the magnitude of dielectric constant.

For $CoFe_2O_4$, the following materials coefficients were used [20–23]: $M_s = 4 \times 10^5\,A\,m^{-1}$, $K_1 = 3 \times 10^5\,J\,m^{-3}$, $K_2 = 0\,J\,m^{-3}$ and $A = 7 \times 10^{-12}\,J\,m^{-1}$ at $T = 25^\circ C$.

For the particular $BaTiO_3$–$CoFe_2O_4$ composite, we can write ε_{ij}^0, the stress-free strain, as

$$\varepsilon_{ij}^0 = \begin{cases} \eta\left[\frac{3}{2}\lambda_{100}\left(m_i m_j - \frac{1}{3}\right)\right] + (1-\eta)\left(Q_{ijkl}P_k P_l\right) & (i=j) \\ \eta\left(\frac{3}{2}\lambda_{111} m_i m_j\right) + (1-\eta) Q_{ijkl} P_k P_l & (i \neq j) \end{cases}, \tag{11}$$

where $Q_{11} = 0.10\,\mathrm{C}^{-2}\,\mathrm{m}^4$, $Q_{12} = -0.034\,\mathrm{C}^{-2}\,\mathrm{m}^4$ and $Q_{44} = 0.029\,\mathrm{C}^{-2}\,\mathrm{m}^4$, and λ_{100} and λ_{111} are the change ratios of the length when magnetized in the (100) and (111) directions, respectively. In this work, $\lambda_{100} = -590 \times 10^{-6}$ and $\lambda_{111} = 120 \times 10^{-6}$. For simplicity, we assumed elastic homogeneity in this work, and the elastic constants of $BaTiO_3$ are used, i.e. $c_{11} = 1.78 \times 10^{11}\,\mathrm{N\,m^{-2}}$, $c_{12} = 0.96 \times 10^{11}\,\mathrm{N\,m^{-2}}$ and $c_{44} = 1.22 \times 10^{11}\,\mathrm{N\,m^{-2}}$.

The temporal evolution of the magnetic domain structure and the ferroelectric domain structure was obtained simultaneously by solving the LLG equation using the Gauss–Seidel projection method [24] for the magnetization and TDGL equation employing the semi-implicit Fourier-spectral method [25] for the polarization. The elastic energy and elastic interactions are obtained using the microelasticity theory of Khachaturyan [26]. The electrostatic energy due to the spatial distribution of electric polarization, magnetostatic interactions due to the magnetic dipole distribution can be obtained using a very similar approach to the elasticity equation.

We assume that the $BaTiO_3$ phase is initially polarized along the z-axis, and the initial magnetization of $CoFe_2O_4$ is chosen to be along the x-axis, as shown in Figure 1b. The 1-3 magnetoelectric composite can be effectively modeled by a two-dimensional (2D) model with periodic boundary conditions if we ignore the polarization inhomogeneity along the rod direction. Most of the simulations presented in this paper were performed in 2D although we also performed a number of 3D simulations for comparison. We fix the volume fraction of $BaTiO_3$ at $\sim$11% for studying the effect of morphology on the domain structures.

4. Domain structures and polarization distributions in the ferroelectric phase

4.1. *Square-shaped ferroelectric particle embedded in a ferromagnetic matrix*

Figure 2a shows a simulated microstructure of the square-shaped rod. We employed a simulation cell of $32\Delta x \times 32\Delta y \times 1\Delta z$ discrete grid points, with the grid spacing of $\Delta x = \Delta y = \Delta z = 1$ nm. In this case, it is equivalent to assuming that the polarization distribution along the z-direction is uniform. We have deliberately chosen a small number of grids, and thus quite small ferroelectric particle size, in order to study vortex formation. As shown in Figure 2a, a double vortex ferroelectric domain structure was observed. The double-vortex structure shows two vortices with different vertical directions: clockwise or anticlockwise. The two vortices share one domain in the middle, in which the polarization is along the same direction as the magnetization orientation in the magnetic phase. We studied the lattice-pinning effect by reducing the grid spacing to $\Delta x = \Delta y = 0.125$ nm, while increasing the number of grid points to 256×256 to maintain the same model size of $32\,\mathrm{nm} \times 32\,\mathrm{nm}$. Interestingly, in this case, at the end of the simulation, only one

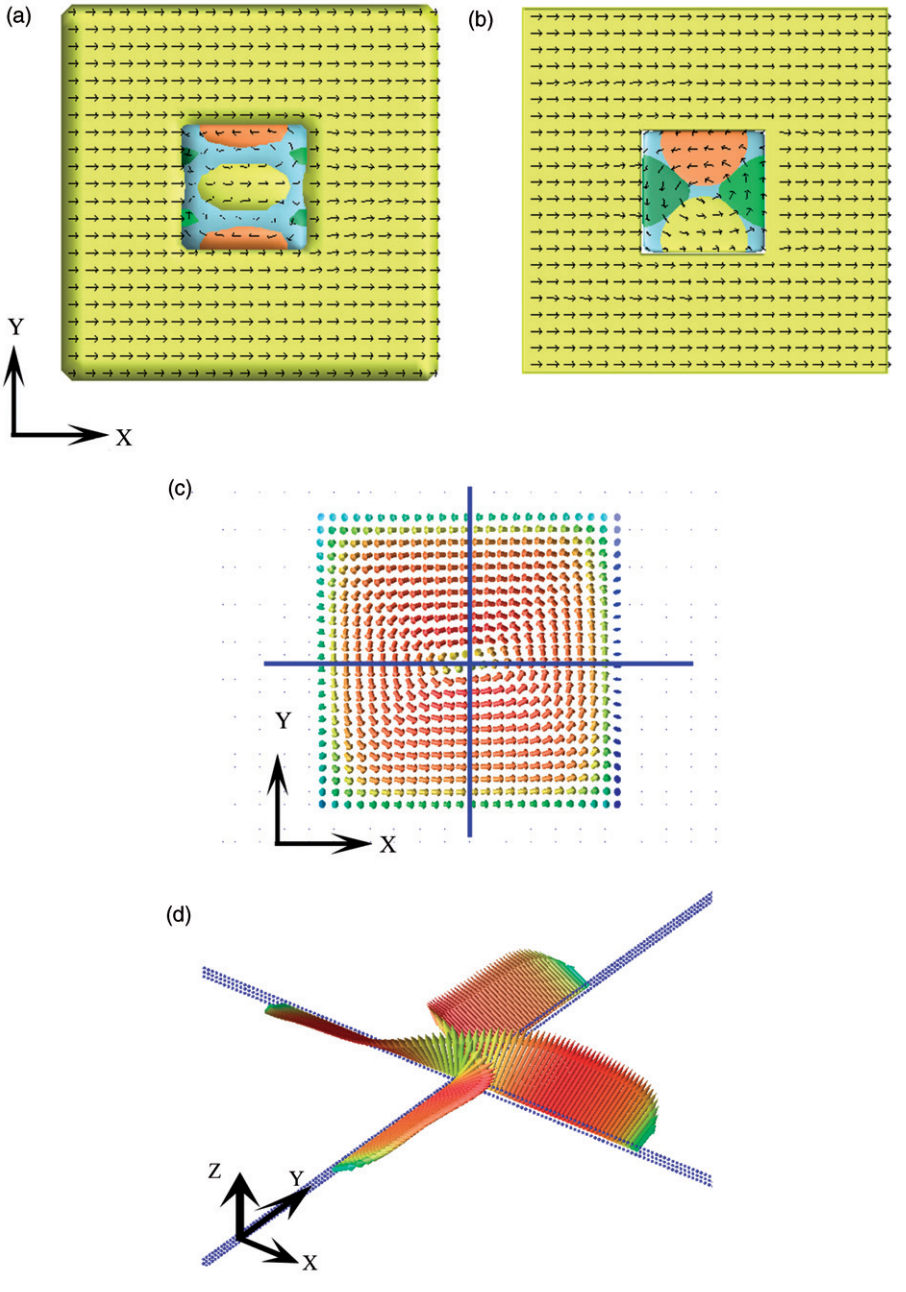

Figure 2. (Color online). Ferroelectric domain structures with a grid spacing of 1 nm (a) and 0.125 nm (b); (c) a 3D vector plot of the ferroelectric phase in (b); (d) the polarization distribution along the *x*- and *y*-axis through the center of (c).

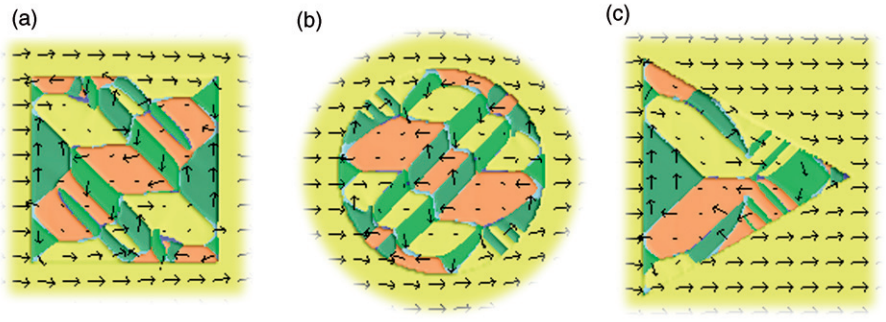

Figure 3. (Color online). The domain structures of multiferroic composite with large grid size, in (a) square-, (b) circle- and (c) triangle-shaped ferroelectric phase.

vortex was observed in the ferroelectric phase, in which four ferroelectric domains were separated by 90° domain walls, as shown in Figure 2b. For better visualization of the polarization distribution of Figure 2b, a vector map of the square-shaped ferroelectric phase is shown in Figure 2c. A group of polarizations near the center of the square is shown in Figure 2d for clarity. It is found that the polarizations only tilted to the x- or y-direction, and the polarizations tilted to opposite directions are connected with a Bloch-type domain wall. As the electrostatic energy is minimized when the polarization is initially polarized along the z-direction, it could not contribute to the polarization tilting. The driving force for the polarization tilting should come from the elastic coupling between the ferroelectric phase and magnetic phase. We observed more polarizations tilted to the direction parallel to the direction of the magnetic phase. This is because the polarization tilted to the x-direction can decrease the elastic energy induced by the magnetostriction.

It should be pointed out that similar polarization vortex patterns have been previously predicted in isolated nanoferroelectrics using a combination of first-principles calculations and an effective Hamiltonian [27–33] and phase-field simulations [34–37], in constrained ferroelectrics by a non-ferroelectric matrix using phase-field simulations [38], and in ferroelectric islands on a substrate [39].

However, such vortex structures are not observed if the ferroelectric particle size is sufficiently large. The domain structures of multiferroic composite with different particle morphology are shown in Figure 3; a simulation cell of $256\Delta x \times 256\Delta y \times 1\Delta z$ discrete grid points was employed with the grid spacing of $\Delta x = \Delta y = \Delta z = 1$ nm. In this case, the particle size is about 85 nm × 85 nm. The ferroelectric domain structures with 90° domain walls are observed in all types of morphology. It should be noted that the ferroelectric domain pattern in the square-shaped and circle-shaped rod exhibit 180° rotation symmetry around the central point, but the triangle-shaped rod exhibits reflection symmetry. The axis of the reflection symmetry is one of the symmetry axes of the regular triangle, and also in the same direction as the magnetization of the surrounding medium. As the magnetic phase is polarized along the x-direction, and the magnetostriction of $CoFe_2O_4$ is negative, a tensile stress is exerted on the ferroelectric phase along the x-direction. For the square- and circle-shaped ferroelectric morphology, the domain pattern exhibits a central symmetry in order to decrease the electric static energy; for the

triangle-shaped ferroelectric phase, there is a tensile stress symmetrically exerted along the x-axis, and hence the ferroelectric phase exhibits axis symmetry.

4.2. *Stability of double-vortex structures*

In order to check the stability of the ferroelectric domain structure shown in Figures 2a and b, we plotted the system free energies as a function of time for the two different grid spacings in Figures 4a and b. It can be seen that for the smaller grid spacing simulation, the ferroelectric polarization initially displays a double-vortex structure (see the inset of Figure 4b). The double-vortex structure remains for a period of time with little change in the total free energy. This double-vortex structure is later transformed to a single vortex with lower free energy. For the case of larger grid spacing (1 nm), the double-vortex structure remains stable throughout the simulation without transforming to single vortex. To determine whether the double-vortex structure with grid spacing of 1 nm is metastable or stable, we also performed a simulation with polarization starting from a random distribution with small values. A single vortex structure was obtained in this case, which has a lower free energy than the double-vortex. (Figure 4a) Therefore, we can conclude that for the case of square-shaped rod, the double-vortex polarization structure is a metastable state.

4.3. *Effect of polarization inhomogeneity along the axial direction*

A 2D model of a 1-3 type ferroelectric rod implies homogeneous distribution along the axial z-direction. To study the effect of inhomogeneity along the axial direction, we performed a 3D simulation using $32 \times 32 \times 32$ grids with grid size 1 nm. We started with a random initial state with small polarizations. The result is presented in Figure 5a. It can be seen that the ferroelectric domain structure in this case is much more complicated. To visualize the polarization distribution more clearly, a vector plot is presented in Figure 5b. It is interesting that the vortex structure appears not only along the x–y plane but also on the x–z plane. A leaf-pattern domain structure is also observed along the y–z plane. Such vortex and leaf-patterns are frequently observed in ferromagnetic domain structures. As the ferroelectric distributions are generally more complex if one starts from a randomly distributed polarization, the following discussions are focused on the initially polarized ferroelectric phase, as in experimental works [12,13].

4.4. *Effect of particle morphology*

Figure 6 shows the simulated polarization distributions in a particle with different morphologies embedded in a magnetic medium, i.e. square, circle and other regular polygons. Vectors represent the projection of the polarization on the x–y plane. As shown in Figure 6, all the ferroelectric phases exhibit vortex structures. A typical characteristic of the vortex structure is that there is a region with the polarization along the z-direction at the center of the vortex structure, which can be observed in all the ferroelectric phases in Figure 6. For polygon-shaped structures, we also notice some regions with the polarization along the z-direction at the vertices (corners) of

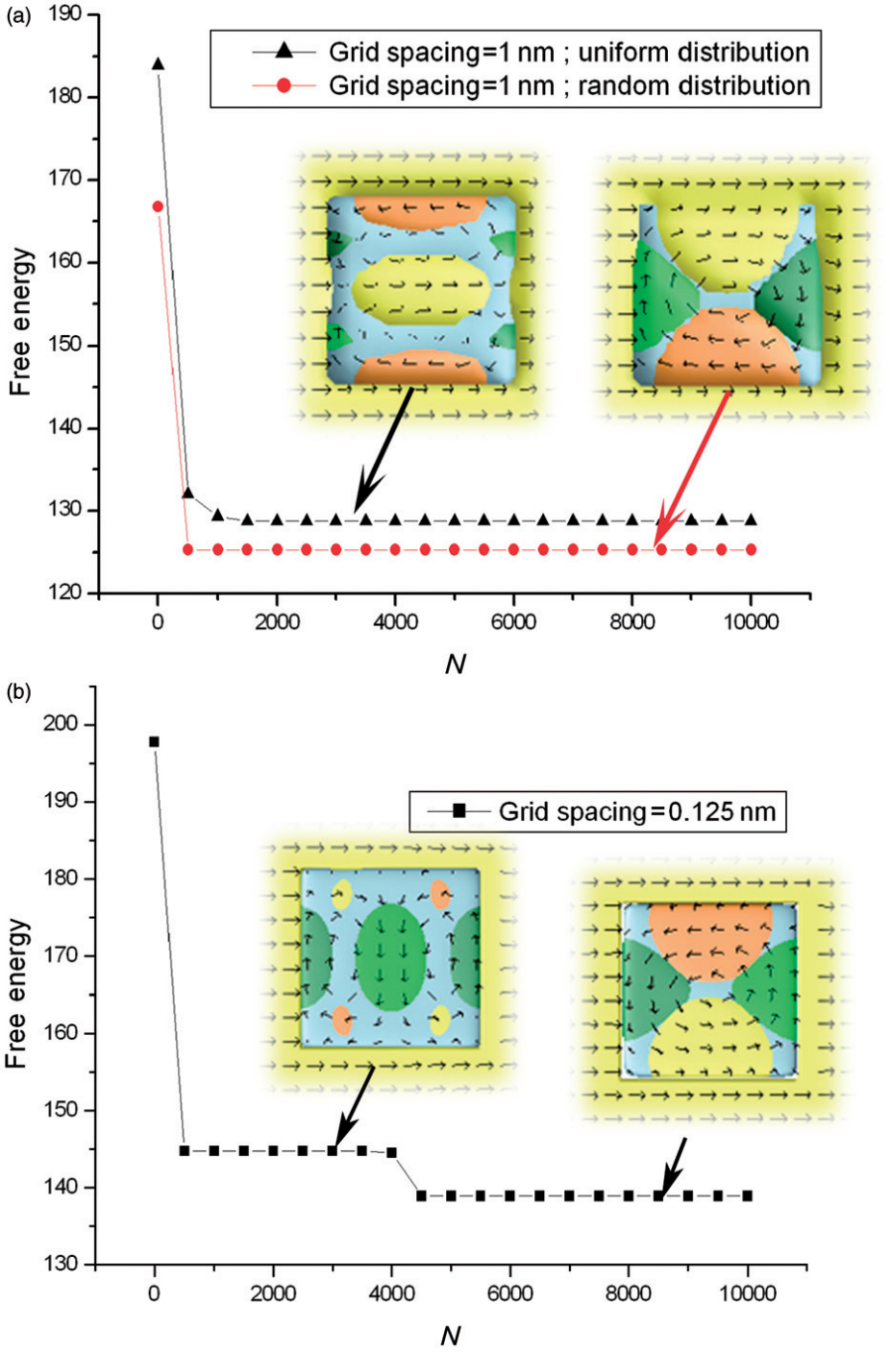

Figure 4. (Color online). The free energy versus $t = N\Delta t$ of square-shaped ferroelectric phase with a grid spacing of 1 nm (a) and 0.125 nm (b).

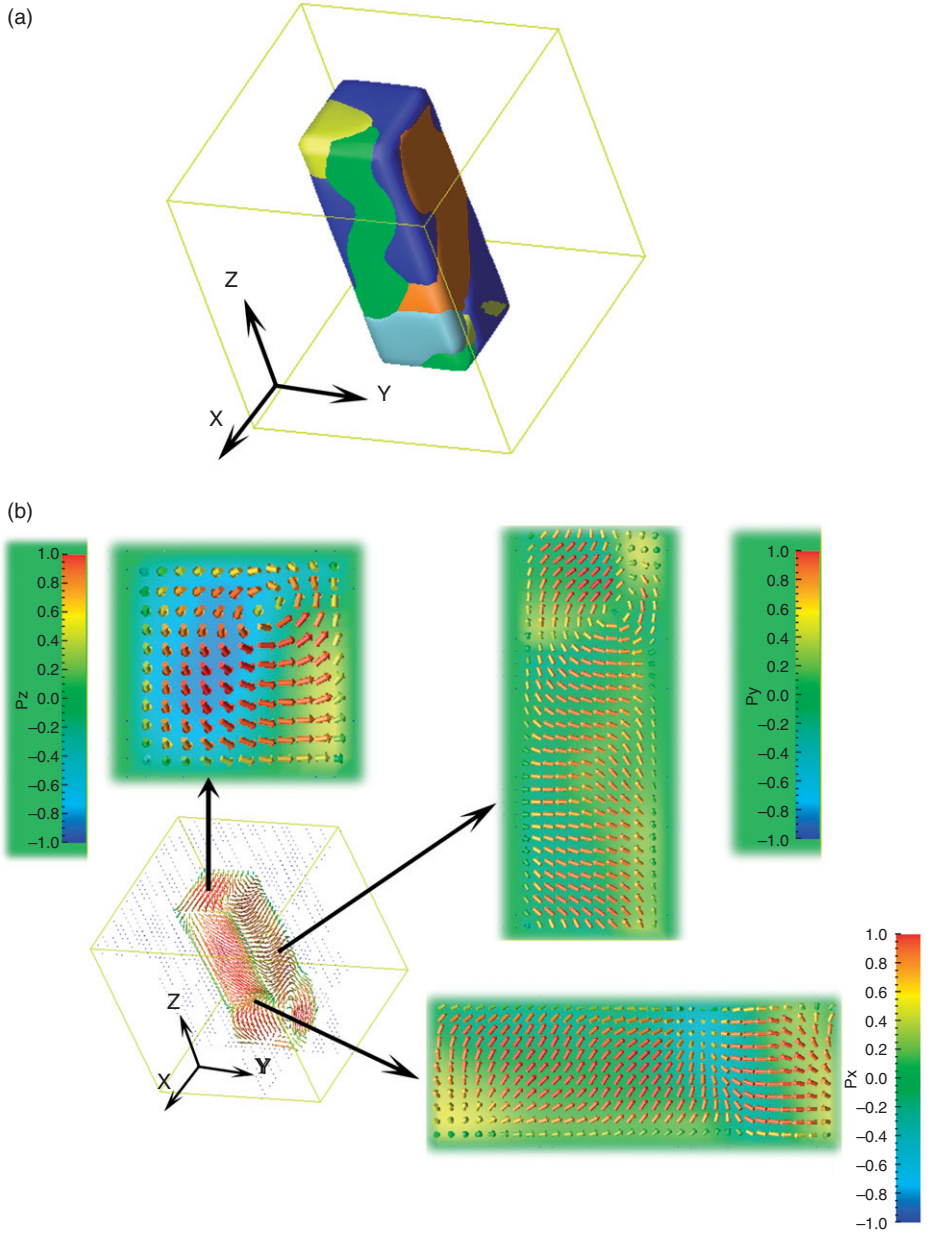

Figure 5. (Color online). (a) The 3D simulation of the ferroelectric domain structure starting from randomly distributed polarization; (b) shows the polarization distributions of (a).

the polygon. The fraction of the region can be influenced by the degree of the interior angle and the orientation of the ferroelectric/magnetic interfaces. For example, the rod with a triangle shape, which has sharp corners, shows larger regions with the polarization along the *z*-direction. Comparing Figures 6a and d, for the same

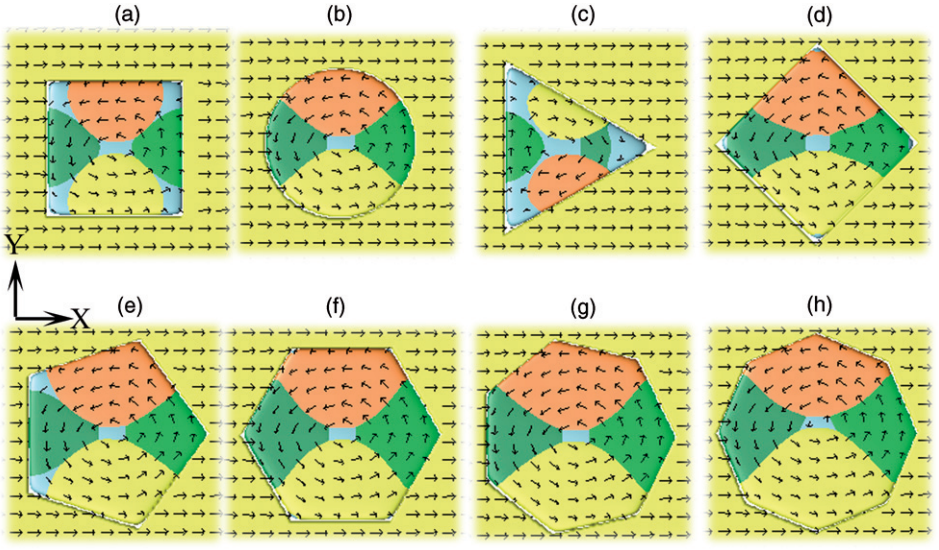

Figure 6. (Color online). Simulated magnetic and ferroelectric domain structures and polarization distribution projected on the x–y plane of the magnetoelectric material: (a) square- and (b) circular-shaped ferroelectric phases; (c–h) polygon-shaped ferroelectric phases.

square-shaped rod, the rod rotates 45° in x–y plane in Figure 6d, and larger regions with the polarization along the z-direction remains at the corners.

We note that during the evolution process of even-sided regular polygon-shaped rods, i.e. regular tetragon-, hexagon- and octagon-shaped rods, the double vortex structures appear as a metastable state. The free energies versus time steps for polygon-shaped rods are plotted in Figure 7. It is shown that for odd-sided polygons, the free energy decreases directly to the minimum corresponding to a single vortex structure, whereas for even-sided polygons, a double vortex structure stays for a period of time with slowly decreasing free energy. Therefore, the appearance of the metastable structure should be related to the symmetry of polygons. The even-sided polygons have a high degree of symmetry, as both the x-axis and y-axis are its symmetric axis, while in the odd side polygons only x-axis is the symmetric axis.

4.5. *Effect of dielectric constants*

There have been a number of discussions with regard to the use of dielectric constants in the time-dependent Ginzburg–Landau model for polarization evolution [40–43]. It is generally agreed that if the polarization in the TDGL model is considered as the spontaneous polarization, a non-vacuum dielectric constant, called ''the background dielectric constant'', should be employed in the electrostatic equilibrium equation [40,41]. On the other hand, if the polarization in a Landau potential is the total polarization, the corresponding dielectric constant in the electrostatic equilibrium equation is the vacuum dielectric constant. Zheng and Woo [43] argued that one should use the spontaneous polarization and background

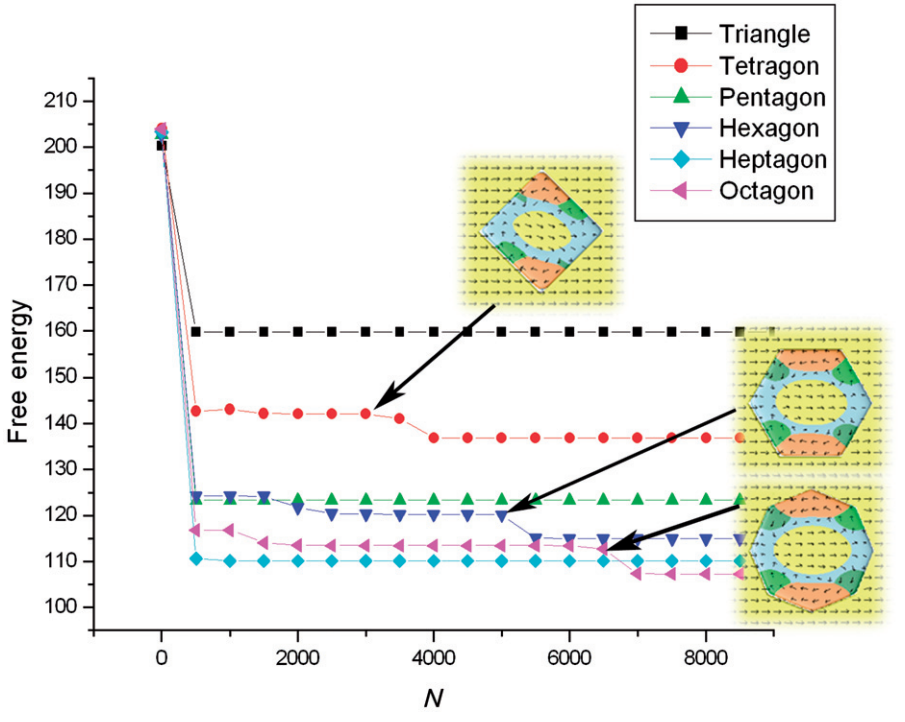

Figure 7. (Color online). Free energy versus $t = N\Delta t$ for different polygons.

dielectric constant to appropriately take into account the depolarization field. The simulation results reported in this paper were obtained by using a dielectric constant of 500. We also performed simulations using small values for the dielectric constant. Figure 8 shows the domain structures using different dielectric constant values. The domain structures of a small particle size of $10\,\text{nm} \times 10\,\text{nm}$ with different grid spacing, 1 nm and 0.125 nm, are shown in Figures 8a and b, respectively. It can be clearly seen that a smaller dielectric constant (i.e. stronger electrostatic interactions or depolarization) leads to more symmetric domain configurations. Even with the order of magnitude difference, for such small ferroelectric particle size, it seems that different values of dielectric constant do not change the main conclusions about the stable single-vortex structure. The effect of dielectric constant on large particles is shown in Figure 8c. In the ferroelectric microstructures, it is obvious that the x domains shrink while the y domains expand with the decrease of the dielectric constant, which is due to the stronger depolarization field and will induce the fraction of x domains and y domains to become more equal at small dielectric constants.

4.6. *Effect of the ferromagnetic matrix*

In order to study the effect of the surrounding magnetic matrix on the polarization distributions, we examined the influence of the magnetization orientation.

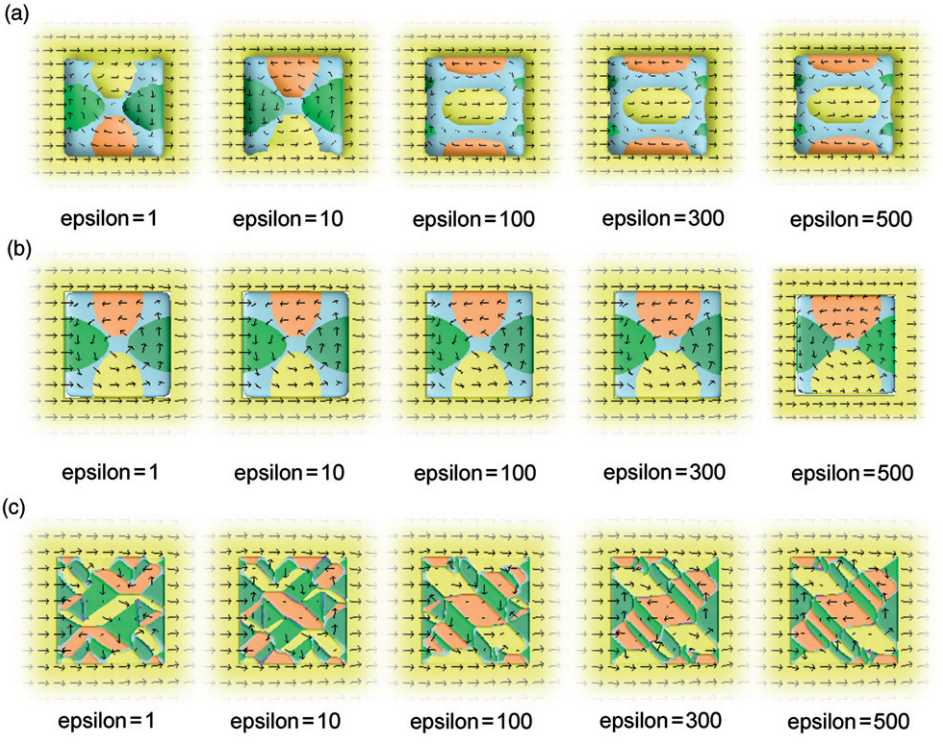

Figure 8. (Color online). The domain structures using different dielectric constant values: (a) a small particle with grid spacing 1 nm; (b) a small particle with grid spacing 0.125 nm; (c) a large particle of 85 nm × 85 nm.

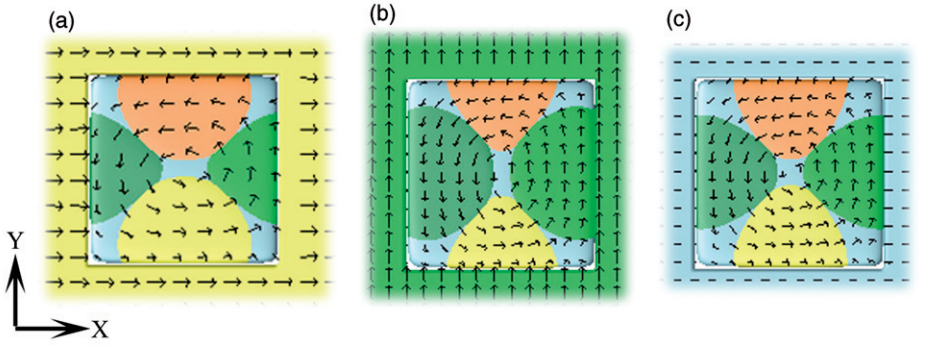

Figure 9. (Color online). The ferroelectric polarization distribution in square-shaped rod with the direction of surrounding magnetic phase along the x-axis (a), then switched to y-axis (b), and z-axis (c).

Figure 9a shows the same polarization distribution in a square-shaped rod. The ferroelectric domains with the polarization along $\pm x$-, $\pm y$-, $\pm z$-directions are labeled as x domain, y domain, z domain, respectively. It is noted that the volume fraction of x domains is clearly larger than y domains. As we switched the

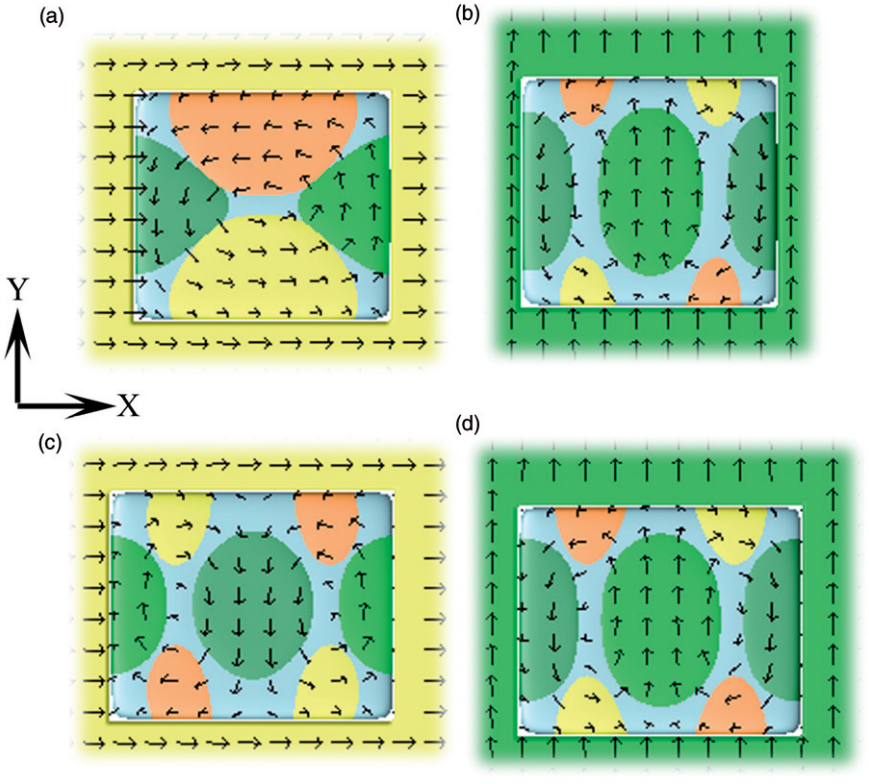

Figure 10. (Color online). (a, b) The aspect ratio = 1.125:1 rectangle-shaped rod, in the magnetic medium along the *x*-axis and *y*-axis, respectively; (c, d) the same for an aspect ratio = 1.25:1.

magnetization direction of the matrix phase to the *y*-direction, as shown in Figure 9b, the volume fraction of *x* domains decreased, whereas that of *y* domains increased. If the magnetization is switched to the *z*-direction, the volume fractions of *x* domains and *y* domains are about the same (Figure 9c). Although the vortex ferroelectric domain structure did not change, we observed a small increase in the volume fraction of *z* domains in Figure 9c. This result shows that the magnetization orientation may influence the stable single-vortex structure, and similar results were also obtained for other ferroelectric particle morphologies.

Since the appearance of metastable double-vortex structure depends on the geometrical symmetry of the ferroelectric rod and the magnetization orientation, we also studied rectangle-shaped rods with different aspect ratios, which are embedded in the magnetic medium with different magnetization orientations. Figures 10a and b show the polarization distributions of a rectangle-shaped rod with aspect ratio = 1.125:1 (length = 12 nm, width = 10.7 nm) with the magnetization in the matrix along the *x*- and *y*-axes, respectively. The results show that, when the magnetization orientation is vertical to the length of the rectangle, the double-vortex structure is stable (Figure 10a). This means the ferroelectric domain structure can be changed by decreasing the degree of symmetry. However, if the direction of the

magnetization is parallel to the length of the rectangle, a single-vortex structure was obtained at the end (Figure 10b). If the aspect ratio is increased to 1.25:1 (length = 13.3 nm, width = 10.7 nm), the double vortex will be stable for both cases, as shown in Figures 10c and d.

5. Summary

We have studied ferroelectric polarization distributions in 1-3 type bulk magneto-electric composites using the phase-field method. We found that, whereas relatively large (~100 nm) single-crystal ferroelectric particles contain normal domain structures, single-vortex polarization structures are formed in small particles (~10 nm) with double-vortex structures appearing as metastable states during evolution towards equilibrium states. The formation of vortex structures and polarization distribution is strongly influenced by the geometrical shapes of the ferroelectric particles and the aspect ratio of rods. It is shown that one can also modify the ferroelectric domain structures by changing magnetization orientation in the magnetic medium. A study on the influence of ferroelectric phase morphology on the magnetoelectric coupling coefficients is currently underway.

Acknowledgements

The authors are grateful for the financial support by the National Science Foundation under the grant number DMR-0507146 and DMR-0820404.

References

[1] M. Fiebig, J. Phys. Appl. Phys. 38 (2005) p.R123.
[2] S. Priya, R. Islam, S. Dong and D. Viehland, J. Electroceram. 19 (2007) p.147.
[3] W. Eerenstein, N.D. Mathur and J.F. Scott, Nature 442 (2006) p.759.
[4] W. Prellier, M.P. Singh and P. Murugavel, J. Phys. Condens. Matter. 17 (2005) p.R803.
[5] C.W. Nan, M.I. Bichurin, S. Dong, D. Viehland and G. Srinivasan, J. Appl. Phys. 103 (2008) p.031101.
[6] G. Harshe, PhD thesis, Pennsylvania State University (1991).
[7] S.X. Dong, J.R. Cheng, J.F. Li and D. Viehland, Appl. Phys. Lett. 83 (2003) p.4812.
[8] J. Ryu, S. Priya, K. Uchino and H. Kim, J. Electroceram. 8 (2002) p.107.
[9] J. Zhai, N. Cai, Z. Shi, Y. Lin and C.W. Nan, J. Appl. Phys. 95 (2004) p.5685.
[10] R.E. Newnham, D.P. Skinner and L.E. Cross, Mater. Res. Bull. 13 (1978) p.525.
[11] H. Zheng, J. Wang, S.E. Lofland, Z. Ma, L. Mohaddes-Ardabili, T. Zhao, L. Salamanca-Riba, S.R. Shinde, S.B. Ogale, F. Bai, D. Viehland, Y. Jia, D.G. Schlom, M. Wuttig, A. Roytburd and R. Ramesh, Science 303 (2004) p.661.
[12] Z. Shi, C.W. Nan, J. Zhang, N. Cai and J.F. Li, Appl. Phys. Lett. 87 (2005) p.012503.
[13] Z. Shi, C.W. Nan, J. Zhang, J. Ma and J.F. Li, J. Appl. Phys. 99 (2006) p.124108.
[14] C.W. Nan, Phys. Rev. B 50 (1994) p.6082.
[15] Y. Ni and A.G. Khachaturyan, J. Appl. Phys. 102 (2007) p.113506.
[16] J.X. Zhang, Y.L. Li, D.G. Schlom, L.Q. Chen, F. Zavaliche, R. Ramesh and Q.X. Jia, Appl. Phys. Lett. 90 (2007) p.052909.
[17] J. Fidler and T. Schrefl, J. Phys. Appl. Phys. 33 (2000) p.R135.

[18] Y.L. Li and L.Q. Chen, Appl. Phys. Lett. 88 (2006) p.072905.
[19] Y.L. Li, L.E. Cross and L.Q. Chen, J. Appl. Phys. 98 (2005) p.064101.
[20] T. Yamada, J. Appl. Phys. 43 (1972) p.328.
[21] Y. Suzuki, R.B. van Dover, E.M. Gyorgy, J.M. Phillips and R.J. Felder, Phys. Rev. B 53 (1996) p.14016.
[22] R.M. Bozorth, E.F. Tilden and A.J. Williams, Phys. Rev. 99 (1955) p.1788.
[23] A.F. Devonshire, Phil. Mag. 42 (1951) p.1065.
[24] X.P. Wang and C.J. Garcia-Cervera, J. Comput. Phys. 171 (2001) p.357.
[25] L.Q. Chen and J. Shen, Comput. Phys. Comm. 108 (1998) p.147.
[26] A.G. Khachaturyan, *Theory of Structural Transfomations in Solid*, Wiley, New York, 1983.
[27] I.I. Naumov, L. Bellaiche and H. Fu, Nature 432 (2004) p.737.
[28] H. Fu and L. Bellaiche, Phys. Rev. Lett. 91 (2003) p.257601.
[29] I. Kornev, H. Fu and L. Bellaiche, Phys. Rev. Lett. 93 (2004) p.196104.
[30] I. Ponomareva, I.I. Naumov and L. Bellaiche, Phys. Rev. B 72 (2005) p.214118.
[31] S. Prosandeev, I. Ponomareva, I. Kornev, I. Naumov and L. Bellaiche, Phys. Rev. Lett. 96 (2006) p.237601.
[32] S. Prosandeev and L. Bellaiche, Phys. Rev. Lett. 97 (2006) p.167601.
[33] S. Prosandeev and L. Bellaiche, Phys. Rev. B 75 (2007) p.094102.
[34] J. Wang and T.Y. Zhang, Appl. Phys. Lett. 88 (2006) p.182904.
[35] J. Wang, M. Kamlah, T.Y. Zhang, Y.L. Li and L.Q. Chen, Appl. Phys. Lett. 92 (2008) p.162905.
[36] Y.C. Shu, J.H. Yen, H.Z. Chen, J.Y. Li and L.J. Li, Appl. Phys. Lett. 92 (2008) p.052909.
[37] L.J. Li, J.Y. Li, Y.C. Shu and J.H. Yen, Appl. Phys. Lett. 93 (2008) p.152906.
[38] J. Slutsker, A. Artemev and A. Roytburd, Phys. Rev. Lett. 100 (2008) p.087602.
[39] J.X. Zhang, R. Wu, S. Choudhury, Y.L. Li, S.Y. Hu and L.Q. Chen, Appl. Phys. Lett. 92 (2008) p.122906.
[40] A.K. Tagantsev, Ferroelectrics 69 (1986) p.321.
[41] V.O. Sherman, A.K. Tagantsev, N. Setter, D. Iddles and T. Price, J. Appl. Phys. 99 (2006) p.074104.
[42] A.L. Roytburd, S. Zhong and S.P. Alpay, Appl. Phys. Lett. 87 (2005) p.092902.
[43] Y. Zheng and C.H. Woo, Appl. Phys. A 97 (2009) p.617.